Nano Energy 62 (2019) 691–699

Contents lists available at ScienceDirect

Nano Energy

journal homepage: www.elsevier.com/locate/nanoen

Full paper

A self-powered multi-broadcasting wireless sensing system realized with an all-in-one triboelectric nanogenerator

Asif Abdullah Khan[a,b], Alam Mahmud[a,b], Steven Zhang[a], Shariful Islam[c], Peter Voss[c], Dayan Ban[a,b,*]

[a] Waterloo Institute for Nanotechnology, University of Waterloo, 200 University Ave West, Waterloo, ON, Canada
[b] Department of Electrical and Computer Engineering, University of Waterloo, 200 University Ave, Waterloo, ON, Canada
[c] Shimco, 75 Heroux Devtek Dr, Cambridge, ON, Canada

ARTICLE INFO

Keywords:
Nanotextures
Triboelectricity
Energy harvesting
Wireless sensing
Multi-broadcast

ABSTRACT

The ubiquitous sensors at the core network of Internet of Things (IoT) have accelerated the realization of micro/nano systems that necessitate not only the development of self-powered sensors but also requires a reliable wireless communication mode. Here, a self-powered multi-broadcasting wireless sensing system based on an all-in-one triboelectric nanogenerator (TENG) is reported, which can simultaneously power up a custom-made wireless node and act as a sensor. The whole device and the system are encapsulated in a unique compact structure, in which the top segment consists of a spring-assisted multifunctional TENG (MTENG) and, the bottom section contains an integrated energy management and Bluetooth transmitter module. Following the structural and material modifications, the top unit of the MTENG is used to detect vibration frequency and amplitude by correlation with the TENG output voltage. The device has been employed to successfully detect the running frequency of a linear shaker and various generated signals. Owing to the nanostructured material surfaces, the device yields an output current of 300 μA and a power density of 4 W/m^2 with the normal hand pressing. Moreover, the developed portable MTENG is also assessed to remotely monitor automobile engine vibration and is expected to result in a myriad of applications.

1. Introduction

In the era of Internet of Things (IoT), the widespread existence of sensors have not only brought great convenience to our lives but has also raised consequential challenges in achieving a wireless sensor network (WSN) with sustainable power supply and reliable wireless communication [1,2]. To power up the distributed sensor nodes in WSNs using batteries is unrealistic since commercial Li-ion batteries have a limited lifetime and the maintenance cost can be prohibitively expensive. An alternative solution is to use an energy-scavenging device in lieu of a Li-ion battery to harvest energy from the ambient environment for sustainable power supply. Over the past decades, various efforts have been devoted to harvest energy from different environmental energy sources such as vibration, water and wind, using electromagnetic [3–7], electrostatic [8–10], and piezoelectric methods [11–14]. Recently, triboelectric nanogenerators (TENGs) based on the coupling effect of contact electrification and electrostatic induction have emerged as a persuasive technology to convert ambient mechanical energy into electric energy with numerous advantages, including large power density, high energy conversion efficiency, versatile options for material selection, light weight, low cost etc. [15–26]. Until now, four modes of TENGs have been significantly investigated – lateral sliding mode, vertical contact-separation mode, freestanding mode, and single-electrode mode. These can scavenge almost all types of mechanical energy from the environment [27–30]. In addition, they have successfully been used as self-powered sensors in wind speed sensing, micro liquid biological and chemical sensing, vibration monitoring, transportation and traffic management, motion tracking, powering biomedical microsystems, among others [31–40]. However, due to the randomness of mechanical energy sources as well as the high internal impedance and low output current of TENGs, their integration with a practical application system is still challenging. After the first demonstration in 2012, there have been remarkable progresses in the device development of TENGs [41,42], but few studies have carefully addressed the efficient integration of a self-powered system [43–46].

In a real-time sensing system, the measured signals need to be processed first, and then transmitted to a central station via one of the different RF techniques, such as wireless local area networks (WLAN),

* Corresponding author.
E-mail address: dban@uwaterloo.ca (D. Ban).

https://doi.org/10.1016/j.nanoen.2019.05.073
Received 26 April 2019; Received in revised form 27 May 2019; Accepted 28 May 2019
Available online 03 June 2019

Cellular, Bluetooth, Zigbee, or Radio-frequency identification (RFID). The inclusion of a signal processing unit and wireless transmission unit imposes a very demanding power supply requirement, given that the power output from most of the energy harvesters under real-life vibration conditions is relatively low. Recently, a self-powered system integrating different function modules was presented, however, it does not incorporate a sensing unit [47]. In another study, although a self-powered system with two separate piezoelectric and triboelectric nanogenerator units enabled transmitting pre-coded signals [48], the low output power from the system may not guarantee sustainable and reliable wireless data transmission.

To address the aforementioned issues, one possible solution can be the development of an all-in-one or multifunctional triboelectric nanogenerator (MTENG), which can simultaneously act a sensor and as energy harvester to operate the whole RF transmitter and signal processor unit. Herein, a self-powered wireless sensing and monitoring system based on a spring-assisted MTENG is proposed and demonstrated to remotely monitor real-time vibration. The designed MTENG works in a vertical contact-separation mode based on triboelectrification between nanostructured polytetrafluoroethylene (PTFE) and aluminum surfaces, which produces output power. Among the eight units that constitute the MTENG, the lower 7 units are connected to the regulated energy management module (EMM) through an embedded full bridge rectifier unit. The EMM can deliver an output voltage of 3.1–3.6 V and a pulsed output current of 100 mA, which can charge a 2.2 mF capacitor to 3 V in 240 s. Vibration signals are collected by the top TENG unit and transmitted wirelessly to multiple receivers in every ~20 s marking a significant step towards real-time deployment for applications such as IoT, structural health monitoring, autonomous vehicles etc. The long-term reliability of the MTENG output and the RF transmission capability is also tested without any interruption for ~38 000 cycles.

2. Material modifications, structural optimization and system design

The self-sustainable wireless vibration monitoring system is composed of an energy harvesting part, a sensing part, and a circuit part. In the sketched MTENG (Fig. 1(a)), each TENG unit consists of a nanostructured Aluminium (Al) foil and Polytetrafluoroethylene (PTFE) as triboelectrically positive and negative layers, respectively. To produce nanostructured PTFE surface, 10 nm gold (Au) was deposited on the PTFE surface by e-beam evaporation to form nanoparticles. The shadowing effect of the thin Au nanoparticles is key to the formation of PTFE nanowire arrays on the surface. ICP (Inductively Coupled Plasma) ionic milling was employed to etch the polymer films with an operation temperature of 55 °C and pressure of 15 mTorr. Fig. 1 a (i) shows the scanning electron microscopy (SEM) image of the PTFE nanostructure surface etched for 2 min. The Al film was immersed in hot deionized (DI) water at 120 °C for 20 min to achieve the desired nanostructures [49]. Fig. 1(a) (ii) shows the SEM image of the etched Al surface, covered uniformly with nanostructures with dimensions less than 200 nm to increase the effective contact area. Finally, a 128 μm thick kapton film was shaped to a zigzag structure by making deformations at the evenly spaced intervals which serves as the substrates for the eight TENG units on both sides as sketched in Fig. 1(a).

The top TENG unit was used for sensing purpose and the rest of the units were used for harvesting mechanical energy. Then the whole device is encapsulated to the top unit of the spring assisted structure as illustrated in Fig. 1 (b, c).

To design the reliable wireless node, the rectified outputs of the seven TENGs were connected to the EMM, to regulate and store the harvested energy, as demonstrated in Fig. 2(a, b). Once the input capacitor was fully charged, an output capacitor was connected to and charged by the input capacitor via the EMM. This two-stage charging system is much more efficient than a single-stage charging system. The RF module was connected to the output capacitor via a linear switching regulator to minimize the leakage current. A discharging level controller of output capacitor based on a delay circuit had been introduced as well to control the data transmission frequency.

Then the high impedance TENG sensor was interfaced with the RF module by an operational amplifier (Op-Amp) based impedance matching unit (IMU) as shown in Fig. 2 (c). The system was pre-set to operate for ~1 s per cycle, during which the measured signal (from the top TENG unit via an impedance matching unit, Fig. 2 (c)) was sampled, digitized and transmitted wirelessly to remote receivers. The designed EMM, the RF module, and the impedance matching unit were integrated on a 1.5 cm × 1.5 cm printed circuit board (PCB) and were placed in the lower segments of the device (Fig. 2 (e, f)). The block diagram of the whole self-powered sensing system is illustrated in Fig. 2 (g). The system was tested under vibration conditions in different contexts: a linear mechanical shaker, a running car, human hand tapping. The experimental results are presented in the following section.

3. Results and discussion

The working principle of each TENG unit is demonstrated in Fig. 3(a). Herein, at first, the contact between the top Al electrode and the PTFE surface creates positive triboelectric charges on the top electrode and negative charges on the PTFE surface (state i). Then the separation between the top electrode and the PTFE film produces a difference in electric potential between the two electrodes, which drives the flow of free electrons from the bottom electrode to the top one (state ii). The current continues until the physical separation reaches the maximum (state iii). When the two surfaces of the top electrode and the bottom PTFE surface get close to each other, the free electrons flow from the top electrode back to the bottom one, thus generating a reverse current (state iv). In order to test the power generation capability of the MTENG, firstly the output voltage was measured with a frequency of ~5 Hz and external force of 7 N applied from a hammer of an electrodynamic shaker and was collected with a TDS 2004C oscilloscope. As shown in Fig. 3(b) the peak-to-peak output voltage from the top TENG unit is ~700 V and the maximum peak output voltage reaches to ~ 400 V. To theoretically validate the result, finite element simulations were performed using COMSOL (Fig. 3 (c)). Based on the electron affinity of PTFE ($-190\,nC\,J^{-1}$) and the applied mechanical force (7 N corresponding to potential energy of ~0.035 J), a maximum surface charge density (MSCD) ~ $6.65\,\mu C\,m^{-2}$ is expected. The MTENG device exhibited a peak output voltage of ~400 V, corresponding to a surface charge density of ~$3.75\,\mu C\,m^{-2}$, which is ~56% of the theoretical MSCD (~$6.65\,\mu C\,m^{-2}$). It was previously reported that triboelectric materials cannot attain the MSCD due to the limitations imposed by air breakdown, thermal fluctuations and humidity in the environment [50].

Then the output current from the device was measured by connecting all TENG units in parallel, and after rectification the average output current reached to ~300 μA with normal hand pressing (Fig. 3 (d)). It can be seen from the output current signal that the rectified output current displays a higher peak followed by a lower peak in each cycle. The higher peak is from pressing motion while the lower one is from releasing motion. This can be explained by the fact that the contact between the two tribo layers, as a result of hand tapping, occurs more rapidly than their separation (due to the slow self-releasing of the kapton substrate). The high output current from the device is attributed to the nanostructured surface modifications of PTFE and Al as well as the proper encapsulation of the device in the kapton substrate. For comparison, another eight-unit TENG device without any surface modifications were fabricated and the measured short circuit current output of this device was only ~150 μA under the same testing condition. The as-fabricated device and its output short circuit current are shown in Fig. S1 and Fig. S2, respectively. The output current fluctuation from one unit to another can be attributed to different motion

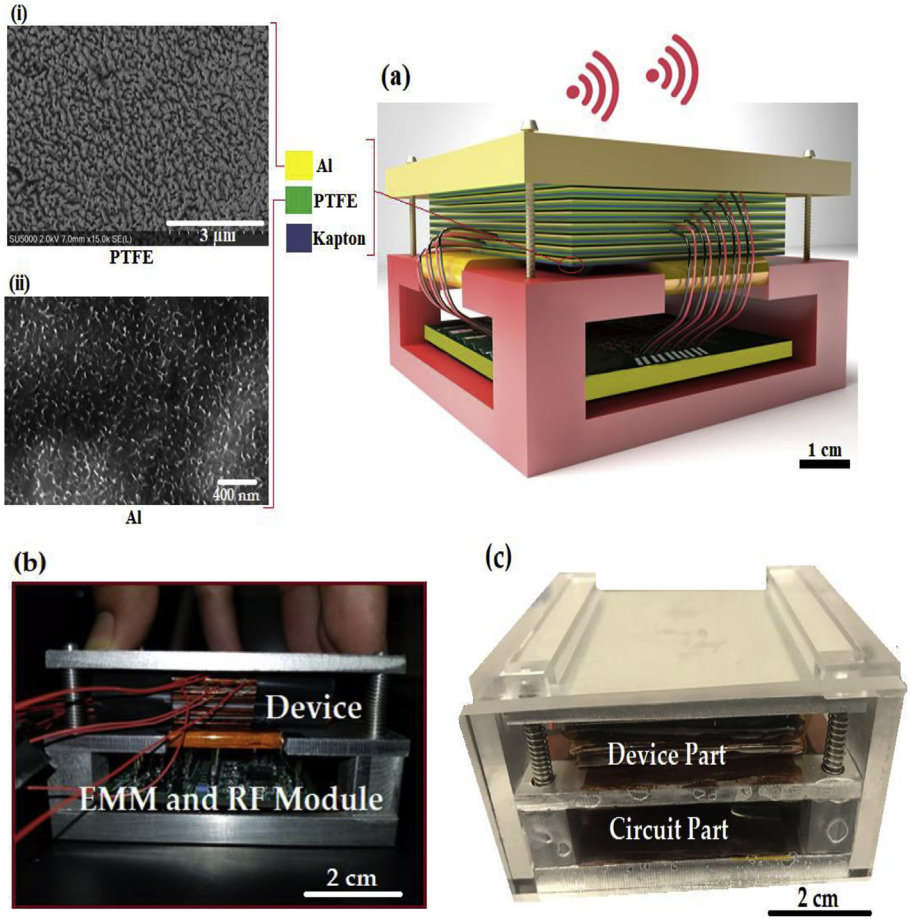

Fig. 1. Structure design of the MTENG (a) Schematic illustration of the functional components of MTENG, which is mainly composed of a TENG units and an integrated circuit unit. (i-ii) Scanning electron microscope (SEM) images of the nanostructured PTFE and Al surfaces. A photograph of (b) an as-fabricated MTENG (before encapsulation with the acrylic) (c) an as-fabricated MTENG (after encapsulation with the acrylic).

states of each TENG unit and non-uniformity of the air gap between them.

Subsequently, different resistors were used to investigate the reliance of the output electric power of MTENG to the external load. The corresponding instantaneous output power as a function of the load resistance ($P = I^2R$) is presented in Fig. 3(e). The maximum output power of ~10 mW and the corresponding power density of ~4 W/m^2 were achieved at a load resistance of 1 MΩ and with a hand-tapping frequency of ~5 Hz, which is sufficient for powering up the whole RF module sustainably. The decrease in the matched resistance of the TENG with eight units compared to the TENG with a single unit is attributed to the increase in total capacitance, according to the matched resistance expression of $1/\omega C$ [51–53].

The effect of the vibration frequency of the linear shaker on the output performance of the MTENG was also investigated. An iron mass of 0.5 kg was attached to the spring-supported top plate of the MTENG and the combined output current was measured with a constant acceleration of 1 g. With 5 mm peak-to-peak vibration displacement from the linear shaker at 10 Hz, the combined output current from the devices was ~30 μA. The output current drops as the frequency increases from 10 Hz to 60 Hz (Fig. 3(f)). The displacement profile of the linear shaker with the same acceleration condition is shown in the inset (i) of Fig. 3(f). The correlation between the short circuit current and the displacement implies that the amplitude of vibration plays a critical role in TENG output performance.

In order to verify the MTENG as the sustainable power source for the wireless sensing, the generated electricity from each TENG unit needs to be stored in different commercial capacitors.

As a higher output voltage level of the input capacitor (C_{IN}) of the EMM can reduce the charging time of the output capacitor (C_{OUT}), the EMM was designed to charge the input capacitor (6.8 μF) up to 16 V, which effectively utilized the high output voltage feature of TENG. Fig. 4(a) displays the charging characteristics of different commercial capacitors with the MTENG up to 3 V. As triggered by hand pressing the charging time of a 2.2 mF, 1 mF and 470 μF capacitors were 240 s, 110 s and 50 s, respectively. Experimental results (Fig. S3) show that the higher energy storage in the input capacitor enhances the energy transfer efficiency to the output capacitor and thus reduces the charging time of the output capacitor significantly. Also, this two stage charging strategy for MTENG was compared with the direct charging method of output capacitor (Fig. S4) and dictated almost 3 times faster charging response.

To calibrate the energy harvesting and data acquisition/transmission of the system, a function generator was employed to produce standard signals to the SoC. A sinusoidal signal and a triangular signal of 1 V peak-to-peak were applied to the SoC input and the whole system was powered by the MTENG instead of any external power source. The received signals are deciphered with a Bluetooth low energy scanner with an amplitude accuracy of ± 0.1 V and also the wave-shape is conserved (Fig. S5). A maximum of 20 sampling points were collected to reconstruct the transferred signal in each RF transmission, where the sampling frequency was set to 650 Hz. The supplementary video 1 and supplementary video 2 demonstrate the full-functioning TENG-powered RF transmission system. While powering up the SoC, the measured voltages across the input capacitor (C_{IN}) and the output capacitor (C_{OUT}) of the EMM are shown in Fig. 4(b).The TENG units start scavenging mechanical energy from the shaking of the linear motor from 12 s, and voltage of the C_{IN} starts to increase (Fig. 4(b)). When the voltage of the input capacitor reaches 16 V, the buck converter is switched on to charge the C_{OUT} and regulates the output voltage to different specific levels. A, B, C, D, E, and F are indicating six different regulated voltage levels of ~0.81 V, ~1.32 V, ~1.76 V, ~2.17 V,

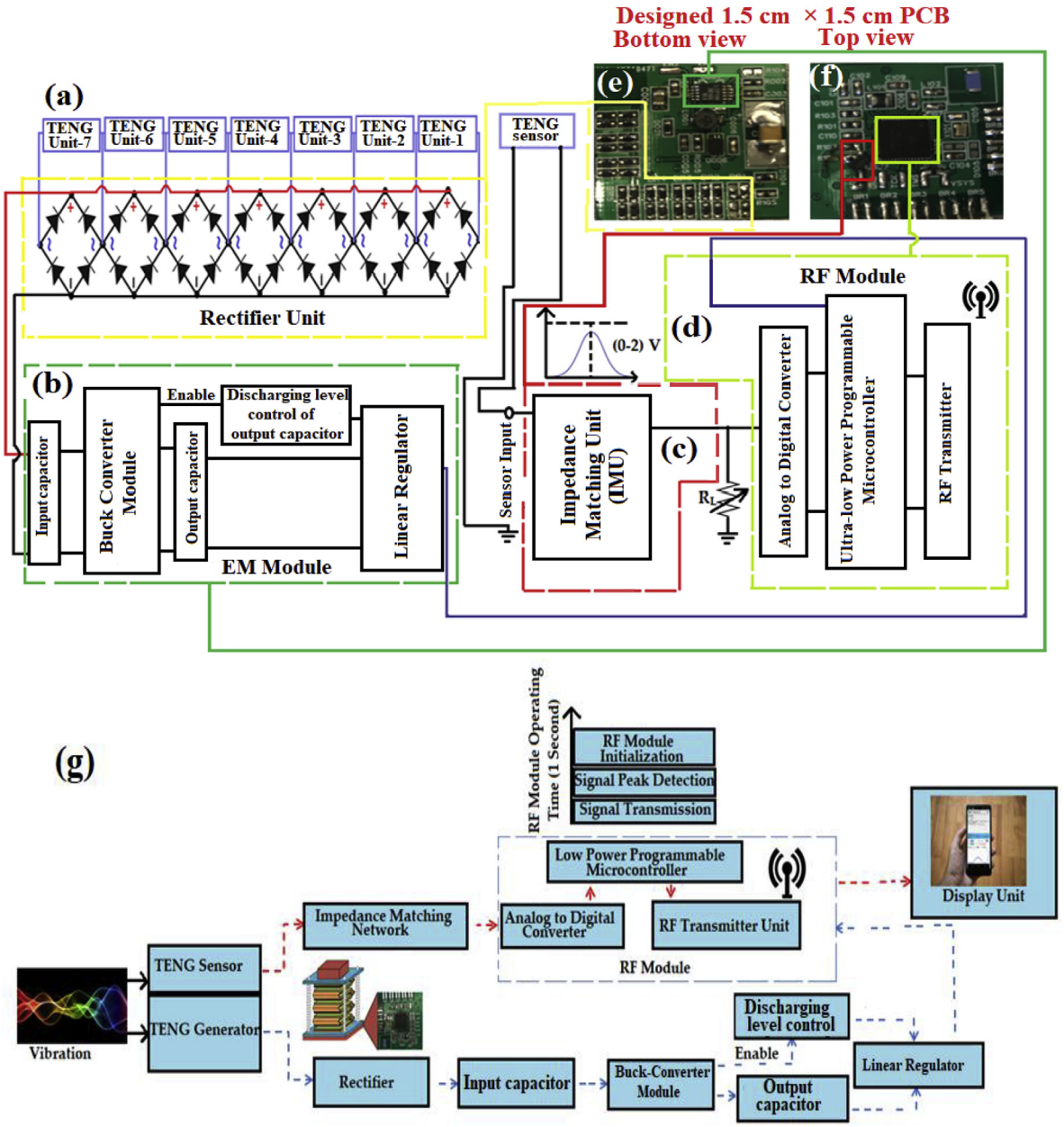

Fig. 2. Design strategy towards achieving an all-in-one MTENG based multi-broadcasting wireless sensing system. (a) Signal rectification units (b) Energy management unit (c) TENG sensor interfacing by impedance matching unit (d) Signal processing and RF module (e–f) Top and bottom view of the manufactured PCB (g) System illustration with the aid of a block diagram.

2.47 V, and ~3.1 V as shown in Fig. 4(d). After the RF module consumes energy from the output capacitor, and voltage of the C_{OUT} drops from 3.1 V to a preset value of ~1 V. In the following cycles; the RF transmission occurs in every ~20 s as the capacitors C_{OUT} and C_{IN} are charged from ~1 V and ~12 V, respectively, rather than from 0 V, as the case in the first cycle. The transferred energy to the output capacitor and received energy by the output capacitor can be calculated by extracting the initial and final values of each peak from Fig. 4(d) as.

Supplementary video related to this article can be found at https://doi.org/10.1016/j.nanoen.2019.05.073.

The calculated transferred energy to the C_{OUT} is 3.15 mJ and the received energy is ~0.8 mJ, which shows an energy transfer efficiency of ~26%. When sending one RF signal, the voltage of C_{OUT} drops from 3.1 V to 1 V within ~1 s working time of the transmitter, corresponding to ~0.2 mW of average power dissipation as shown in Fig. S6. The more detailed theoretical analysis on energy transfer efficiency and power consumption calculation has been presented in the supplementary information section (see section J).

Following the demonstration with the mimic signals, top TENG unit was used as a sensor to collect the real vibration signals to be transmitted wirelessly. Therefore, before integrating the TENG sensor with the SoC, output voltages were also measured under the vibration of the linear shaker at 1 g acceleration and with the frequencies of 10, 15 and 20 Hz and corresponding peak-to-peak output voltages are illustrated in Fig. 4 (e). The gradual decrease in output voltage depicts the reduction of mechanical displacement of the linear shaker with the increase in frequency which in turns weakens the contact electrification process. The optimum frequency of the MTENG is.

Determined primarily by the spring supported structure and the output performance is higher at a lower frequency, which may comply with the resonant frequency (~2 Hz) of the device.

Fig. 5 (a) illustrates the experimental arrangement with the MTENG

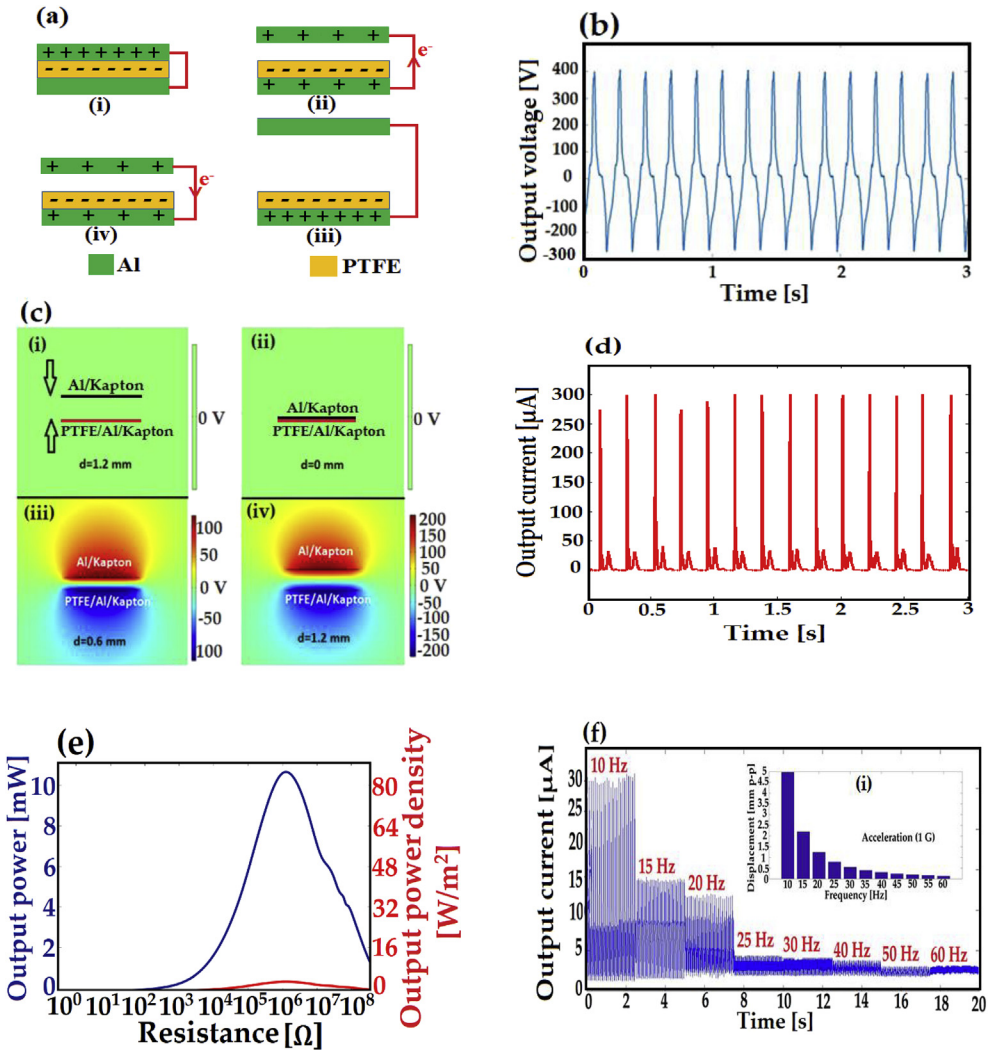

Fig. 3. Theoretical simulation and output performance of the multifunctional TENG (a) Schematic diagram showing the working principle of the MTENG. (b) Simulated potential distribution of the MTENG at four different displacement condition (i-iv) by COMSOL software. (c–d) Measured output voltage and rectified short-circuit current of the MTENG with a frequency of ~5 Hz. (e) Measured output power of the MTENG with a frequency of ~5 Hz and applied force of ~7 N. (f) Comparison of the rectified output current at different frequency excitation of a linear motor (Inset (i) showing the displacement variation of the linear motor with different frequencies.

on top of the linear shaker running at a frequency of 20 Hz and 1 g acceleration. Here, the MTENG has been utilized to detect oscillation frequency of the linear motor by seeking the peak amplitude from the TENG sensor output. Any smartphones can be employed to receive this sensor information wirelessly, that will indicates the peak amplitude and frequency of the TENG sensor output. As triggered by the oscillation of the shaker, MTENG empowers the output capacitor and wirelessly transmits the sensor signals. The received signals which are deciphered by Bluetooth low energy (BLE) scanner, indicates a peak value of 1.48 V (Fig. 5 (a)), which is close to the maximum value of the TENG sensor before the transmission begins (Fig. 4 (e)). As the analog to digital converter of the SoC allows only the positive value of the signal input, the TENG sensor output is rectified by a single diode to allow only the positive half cycle to be transmitted to the mobile receiver. The pulse width in the smartphone display provides the number of sampling points used to represent the positive half cycle of sensor output, which is used to identify the frequency from the correlation with the ADC sampling rate. Within half of a pulse period in the received signal, the number of the sampling points is counted to be $N = 17$ (Fig. 5 (a)), which is used to calculate the pulse frequency as $(N/650)^{-1}/2 = 19.1 \pm 1.1$ Hz. This is very close to the real vibration frequency of the electrodynamic shaker (20 Hz) in this test.

Furthermore, to verify the multi-broadcasting capability of the MTENG, it was used to successfully scavenge biomechanical energy to power up the whole SoC (Fig. 5(b)). The supplementary video 3 demonstrates the wirelessly transmitted TENG sensor signals received by multiple smartphones within ~15 s of hand tapping with an average frequency of ~5 Hz. As for low-frequency applications (< 10 Hz), the signal digitization sampling rate could be tuned higher so that the extracted frequency after data transmission can be more accurate.

Finally, the device was used for harnessing energy from a running and vibrating automobile engine. The device was placed and fixed between the yellow crash bar and the engine to effectively harvest energy from the engine vibration (Fig. 5(c)). To isolate the device from the heat generated by the engine, a thick insulating layer of foam was inserted between the device and the engine. The scanning time of the BLE scanner was set to a longer period of around 30 min, so that wireless data transmitted by the MTENG is not unnoticed. As the engine started, the spring-assisted free moving top plates pushed the device in an up-down direction and after running the car almost ~15 min, the device transmitted the sensor signal wirelessly to the receiver. The corresponding outdoor received signal by the smart phone receiver is demonstrated in Fig. 5(c). This successfully demonstrates the potential deployment of this prototype system in a real application scenario – harvesting sufficient energy from automobile engine vibration for wireless data transmission. The reliability of the MTENG was also carefully studied at a frequency of 10 Hz and an acceleration of 1 g, which shows negligible decrease of output over ~38000 cycles of operation (Fig. S7). Despite of indoor reflection and shielding, the receiver was also able to receive wirelessly transmitted sensor information at a distance of up to 12 m (Fig. S8).

Supplementary video related to this article can be found at https://

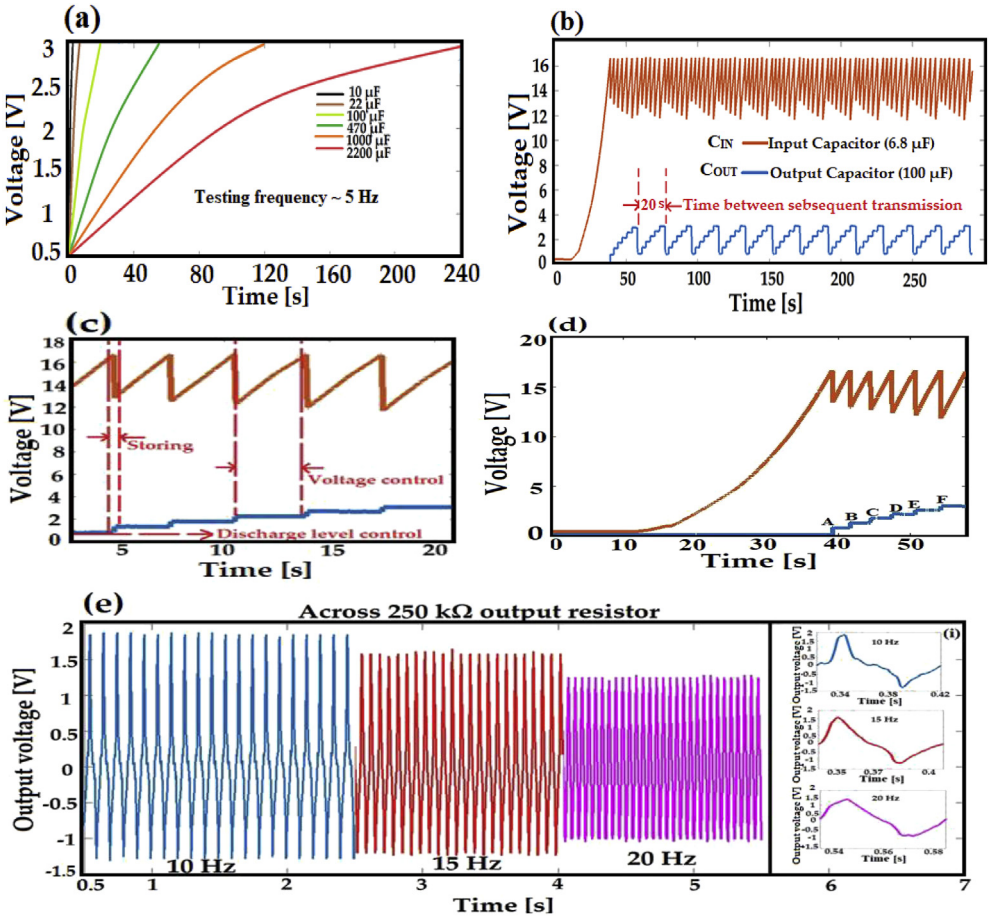

Fig. 4. The charging capability of the MTENG to drive the wireless node and sensing characteristics optimization. (a) The measured output voltage across various commercial capacitors, charged by the MTENG, while triggered by hand tapping. (b) Measured output voltage across the input and output capacitor of the EMM, when the SoC is connected with it and MTENG is excited with the shaking of the linear motor running at 10 Hz. (c–d) close-up view of the measured waveforms in Fig. 4(b), is indicating voltage controlled two stage charging strategy. (e) The output voltage of the top TENG unit at a resistance of 250 kΩ and with different frequencies.

doi.org/10.1016/j.nanoen.2019.05.073.

4. Conclusions

In summary, we present an all-in-one nanostructure-based integrated multifunctional TENG with an improved structural design to develop a self-powered multi-broadcasting wireless sensing system. The fabricated MTENG can produce a high output current of up to ~300 µA and output power of ~10 mW by scavenging ambient mechanical energy. Different commercial capacitors can be charged to 3–3.6 V in a highly efficient way through an optimized energy management module (EMM). Through the innovative structural design of the MTENG, and the correlation of output with the ambient vibration frequency, it can be utilized as a vibration sensor and as energy harvester units; the EMM unit collects, stores and manages the generated electrical energy; a RF wireless module is then powered to transmit the vibration signal to multiple receivers simultaneously. The self-powered system can sense and transmit the vibration amplitude and frequency of a linear mechanical shaker up to a distance of 12 m in every ~20 s. Moreover, the whole functions of the self-powered prototype system has been validated under different application scenarios including running vehicles, biomechanical motion etc. This system can be further modified with multiple permanent storages to power up many wireless nodes. This direct integration of the TENG devices with a Bluetooth supported SoC will benefit a myriad of applications, especially in structural health monitoring, automobile engine vibration monitoring, and biomechanical applications.

5. Experimental section

Nanostructured surface preparation: Each TENG unit consists of a nanostructured Al foil and Polytetrafluoroethylene (PTFE) as triboelectrically positive and negative layers. For producing a nanostructured PTFE surface, 10 nm gold (Au) was deposited on PTFE surface by e-beam evaporation and shadowing effect of the thin Au nanoparticles was employed as a key to the formation of PTFE nanowire arrays on the surface. We used ICP (Inductively Coupled Plasma) ionic milling to etch the polymer films by using Ar, O_2, and CF_4 as the etching gases. After the nanoscale masking with the Au nanoparticles on the PTFE surface, Ar, O_2 and CF_4 gases were introduced into the ICP chamber with the flow ratios of 15.0, 10.0 and 30.0 sccm (standard cubic centimeter per minute), respectively. The operation temperature was 55 °C with a pressure of 15 mTorr. For generating a large density of the plasma, the AC power of 400 W was used while the DC power of 100 W was used to accelerate the plasma ions towards the PTFE surface. After 2 min of etching, the nanostructure is shown in Fig. 1(a–i) was achieved. To increase the effective contact area of the Al film the surface was etched into nanostructures by using a simple method, whereby the Al film was immersed in hot deionized water at 120 °C for 20 min, as described in detail elsewhere [49].

Fabrication of the all-in-one TENG: The length and width of the MTENG package is 6.5 cm × 6.5 cm having 2 cm of total height. The structure contains two units; the top unit is containing the TENG units and the bottom unit contains the circuits. As shown in Fig. 1(a), the mechanical structure was made of three aluminum plates of 6.5 cm × 6.5 cm × 0.5 cm. Four aluminum blocks with a height of 0.5 cm were attached to the bottom plate to support the middle plate. Another four iron bars with a height of 2.2 cm were inserted through the aluminum blocks to reinforce the top plate. The top plate was designed to remain flexible by coiling the iron bars with four springs. Each of the spring has a spring constant of 0.07 lb/inch.

The device is sandwiched between the top and middle plate while

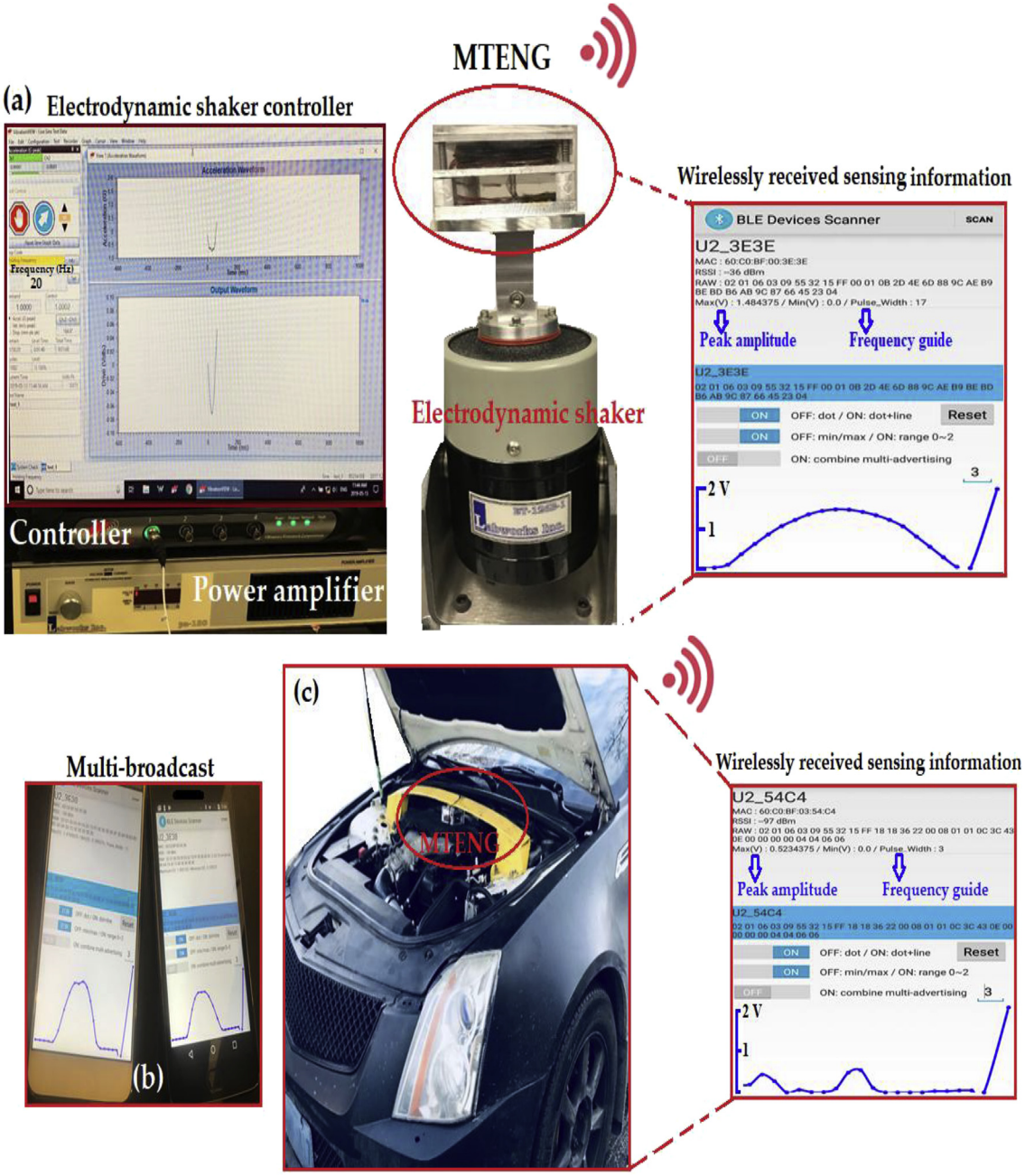

Fig. 5. Application of the MTENG (a) The photograph is showing the wireless sensing application of MTENG, harnessing energy from the vibration of an electrodynamic shaker, running at a frequency of 20 Hz and an acceleration of 1 G. (b) The Photograph is demonstrating the multi-broadcasting of TENG sensor information to various smartphones, when triggered by hand tapping. (c) The MTENG harvesting energy from automobile engine vibration and transmitting the sensor signal wirelessly to the remote receiver.

bottom unit remains immovable due to the fixed aluminum blocks in order to carry the rectification unit, EMM module and RF module. In addition, the middle plate is covered with 120 μm thick kapton insulator to provide proper electrical isolation for the device. Finally, four acrylic sheets with 0.5 cm thickness were attached with each sides of the device which serves as a protecting shield as well as a stopper for the top plate.

Circuit design: An integrated printed circuit board of 1.5 cm × 1.5 cm was designed, which includes eight rectification units, an energy management unit, and a signal processing and transmission unit (RF module) ((Fig. 2)). The rectified output currents from the parallelly-connected TENGs are used to store in the input capacitor of the EMM to charge the output capacitor more efficiently. The linear regulator module in the EMM is used as a switch to power the RF module when the output voltage of the output capacitor reaches its regulation point and is enabled till the logic level reaches 92% of its peak value. In order to control the discharging level of the output capacitor, a 0.1 μF capacitor in parallel with 8 MΩ resistor was connected with the logic line of the EMM module through a diode that determines the discharging time. The EMM is connected with the RF module which is a programmable system on chip and supported by the Bluetooth technology. The TENG sensor is integrated with the SoC through an Op-Amp based impedance matching unit. The designed RF module is set to operate 1 s and used to find the sensor peak value by comparing up to 100 sample points within the set time, which is also crucial for the power consumption of the microprocessor. The threshold for the

comparison between the sample points is set to 200 mV to investigate the peak amplitude of the TENG sensor and the sampling frequency is fixed at 650 Hz for the specific case study.

Acknowledgements

This research was financially supported by The Natural Sciences and Engineering Research Council of Canada (NSERC) and Ontario Centres of Excellence. The authors thank Giga-to-Nano Electronices (G2N) lab for the experiment facilities, and Dr. Md. Golam Kibria for helpful discussions.

Appendix A. Supplementary data

Supplementary data to this article can be found online at https://doi.org/10.1016/j.nanoen.2019.05.073.

References

[1] P. Kamalinejad, C. Mahapatra, Z. Sheng, S. Mirabbasi, V.C.M. Leung, Y.L. Guan, Wireless energy harvesting for the Internet of things, IEEE Commun. Mag. 53 (2015) 102–108.
[2] D. Miorandi, S. Sicari, F. De Pellegrin, I. Chlamtac, Internet of things: vision, applications and research challenges, Ad Hoc Netw. 10 (2012) 1497–1516.
[3] S.J. Park, S.H. Lee, M.L. Seol, S.B. Jeon, H. Bae, D. Kim, G.H. Cho, Y.K. Choi, Self-sustainable wind speed sensor system with omnidirectional wind based triboelectric generator, Nano Energy 55 (2019) 115–122.
[4] T.X. Xiao, X. Liang, T. Jiang, L. Xu, J.J. Shao, J.H. Nie, Y. Bai, W. Zhong, Z.L. Wang, Spherical triboelectric nanogenerators based on spring-assisted multilayered structure for efficient water wave energy harvesting, Adv. Funct. Mater. 28 (2018) 1802634.
[5] I. Sari, T. Balkan, H. Kulah, An electromagnetic micro power generator for wide-band environmental vibrations, Sens. Actuators A Phys. 145 (2008) 405–413.
[6] C.R. Saha, T. O' Donnell, N. Wang, P. McCloskey, Electromagnetic generator for harvesting energy from human motion, Sens. Actuators A Phys. 147 (2008) 248–253.
[7] S.P. Beeby, R.N. Torah, M.J. Tudor, P. Glynne-Jones, T. O'Donnell, C.R. Saha, S. Roy, A micro electromagnetic generator for vibration energy harvesting, J. Micromech. Microeng. 17 (2007) 1257–1265.
[8] P.D. Mitcheson, P. Miao, B.H. Stark, E.M. Yeatman, A.S. Holmes, T.C. Green, MEMS electrostatic micropower generator for low frequency operation, Sens. Actuators A Phys. 115 (2004) 523–529.
[9] H. Tian, S. Ma, H.M. Zhao, C. Wu, J. Ge, D. Xie, Y. Yang, T.L. Ren, Flexible electrostatic nanogenerator using graphene oxide film, Nanoscale 5 (2013) 8951–8957.
[10] Z.L. Wang, J. Song, Piezoelectric nanogenerators based on zinc oxide nanowire arrays, Science 312 (2006) 242–246.
[11] M.P. Lu, J. Song, M.Y. Lu, M.T. Chen, Y. Gao, L.J. Chen, Z.L. Wang, Piezoelectric nanogenerator using p-type ZnO nanowire arrays, Nano Lett. 9 (2009) 1223–1227.
[12] M.L. Seol, H. Im, D.I. Moon, J.H. Woo, D. Kim, S.J. Choi, Y.K. Choi, Design Strategy for a piezoelectric nanogenerator with a well-ordered nanoshell array, ACS Nano 7 (2013) 10773–10779.
[13] A. Mahmud, A.A. Khan, P. Voss, T. Das, E.A. Rahman, D. Ban, A high performance and consolidated piezoelectric energy harvester based on 1D/2D hybrid zinc oxide nanostructures, Adv. Mater. Interfaces 5 (2018) 1801167.
[14] A.A. Khan, A. Mahmud, D. Ban, Evolution from single to hybrid nanogenerator: a contemporary review on multimode energy harvesting for self-powered electronics, IEEE Trans. Nanotechnol. 18 (2019) 21–36.
[15] F.R. Fan, Z.Q. Tian, Z.L. Wang, Flexible triboelectric generator, Nano Energy 1 (2012) 328.
[16] T. Jiang, X. Chen, C.B. Han, W. Tang, Z.L. Wang, Theoretical study of rotary free-standing triboelectric nanogenerators, Adv. Funct. Mater. 25 (2015) 2928.
[17] Y. Yao, T. Jiang, L. Zhang, X. Chen, Z. Gao, Z.L. Wang, Charging system optimization of triboelectric nanogenerator for water wave energy harvesting and storage, ACS Appl. Mater. Interfaces 8 (2016) 21398–21406.
[18] Z.L. Wang, T. Jiang, L. Xu, Toward the blue energy dream by triboelectric nanogenerator networks, Nano Energy 39 (2017) 9–23.
[19] J. Nie, Z. Ren, J. Shao, C. Deng, L. Xu, X. Chen, M. Li, Z.L. Wang, Self-powered microfluidic transport system based on triboelectric nanogenerator and electrowetting technique, ACS Nano 12 (2018) 491–1499.
[20] Y. Bai, C.B. Han, C. He, G.Q. Gu, J.H. Nie, J.J. Shao, T.X. Xiao, C.R. Deng, Z.L. Wang, Washable multilayer triboelectric air filter for efficient particulate matter $PM_{2.5}$ removal, Adv. Funct. Mater. 28 (2018) 1706680.
[21] X. Cao, M. Zhang, J. Huang, T. Jiang, J. Zou, N. Wang, Z.L. Wang, Inductor-free wireless energy delivery via maxwell's displacement current from an electrodeless triboelectric nanogenerator, Adv. Mater. 30 (2018) 1704077.
[22] D.H. Kim, H.J. Shin, H. Lee, C.K. Jeong, H. Park, G.T. Hwang, H.Y. Lee, D.J. Joe, J.H. Han, S.H. Lee, J. Kim, B. Joung, K.J. Lee, In vivo self-powered wireless transmission using biocompatible flexible energy harvesters, Adv. Funct. Mater. 27 (2017) 1700341.
[23] H.S. Wang, C.K. Jeong, M.H. Seo, D.J. Joe, J.H. Han, J.B. Yoon, K.J. Lee, Performance-enhanced triboelectric nanogenerator enabled by wafer-scale nanogrates of multistep pattern downscaling, Nano Energy 35 (2017) 415–423.
[24] S. Li, J. Wang, W. Peng, L. Lin, Y. Zi, S. Wang, G. Zhang, Z.L. Wang, Sustainable energy source for wearable electronics based on multilayer elastomeric triboelectric nanogenerators, Adv. Energy Mater. 7 (2017) 1602832.
[25] S.S.K. Mallineni, Y. Dong, H. Behlow, A.M. Rao, R. Podila, A wireless triboelectric nanogenerator, Adv. Energy Mater. 8 (2018) 1702736.
[26] W. Liu, Z. Wang, G. Wang, G. Liu, J. Chen, X. Pu, Y. Xi, X. Wang, H. Guo, C. Hu, Z.L. Wang, Integrated charge excitation triboelectric nanogenerator, Nat. Commun. 10 (2019) 1426.
[27] Y. Dong, S.S.K. Mallineni, K. Maleski, H. Behlow, V.N. Mochalin, A.M. Rao, Y. Gogotsi, R. Podila, Metallic MXenes: a new family of materials for flexible triboelectric nanogenerators, Nano Energy 44 (2018) 103–110.
[28] S. Niu, Y. Liu, X. Chen, S. Wang, Y.S. Zhou, L. Lin, Y. Xie, Z.L. Wang, Theory of freestanding triboelectric-layer-based nanogenerators, Nano Energy 12 (2015) 760–774.
[29] Z.L. Wang, Triboelectric nanogenerators as new energy technology for self-powered systems and as active mechanical and chemical sensors, ACS Nano 7 (2013) 9533–9557.
[30] Y. Zi, S. Niu, J. Wang, Z. Wen, W. Tang, Z.L. Wang, Standards and figure-of-merits for quantifying the performance of triboelectric nanogenerators, Nat. Commun. 6 (2015) 8376.
[31] W. Yin, Y. Xie, J. Long, P. Zhao, J. Chen, J. Luo, X. Wang, S. Dong, A self-powered transmission and non-contact-reception keyboard based on a novel resonant triboelectric nanogenerator (R-TENG), Nano Energy 50 (2018) 16–24.
[32] H. Yu, X. He, W. Ding, Y. Hu, D. Yang, S. Lu, C. Wu, H. Zou, R. Liu, C. Lu, Z.L. Wang, A self-powered dynamic displacement monitoring system based on triboelectric accelerometer, Adv. Energy Mater. 7 (2017) 1700565.
[33] J. Chen, P. Ding, R. Pan, W. Xuan, D. Guo, Z. Ye, W. Yin, H. Jin, X. Wang, S. Dong, J. Luo, Self-powered transparent glass-based single electrode triboelectric motion tracking sensor array, Nano Energy 34 (2017) 442–448.
[34] S. Lee, R. Hinchet, Y. Lee, Y. Yang, Z. Lin, G. Ardila, L. Montès, M. Mouis, Z.L. Wang, Ultrathin nanogenerators as self-powered/active skin sensors for tracking eye ball motion, Adv. Funct. Mater. 24 (2014) 1163.
[35] Y. Ma, Q. Zheng, Y. Liu, B. Shi, X. Xue, W. Ji, Z. Liu, Y. Jin, Y. Zou, Z. An, W. Zhang, X. Wang, W. Jiang, Z. Xu, Z.L. Wang, Z. Li, H. Zhang, Self-powered, one-stop, and multifunctional implantable triboelectric active sensor for real-time biomedical monitoring, Nano Lett. 16 (2016) 6042–6051.
[36] X. Pu, H. Guo, J. Chen, X. Wang, Y. Xi, C. Hu, Z.L. Wang, Eye motion triggered self-powered mechnosensational communication system using triboelectric nanogenerator, Sci. Adv. 3 (2017) 1700694.
[37] Y. Su, G. Zhu, W. Yang, J. Yang, J. Chen, Q. Jing, Z. Wu, Y. Jiang, Z.L. Wang, Triboelectric sensor for self-powered tracking of object motion inside tubing, ACS Nano 8 (2014) 3843–3850.
[38] B. Zhang, J. Chen, L. Jin, W. Deng, L. Zhang, H. Zhang, M. Zhu, W. Yang, Z.L. Wang, Rotating-disk-based hybridized electromagnetic–triboelectric nanogenerator for sustainably powering wireless traffic volume sensors, ACS Nano 10 (2016) 6241–6247.
[39] X. Chen, Y. Song, Z. Su, H. Chen, X. Cheng, J. Zhang, M. Han, H. Zhang, Flexible fiber-based hybrid nanogenerator for biomechanical energy harvesting and physiological monitoring, Nano Energy 38 (2017) 43–50.
[40] B. Zhang, L. Zhang, W. Deng, L. Jin, F. Chun, H. Pan, B. Gu, H. Zhang, Z. Lv, W. Yang, Z.L. Wang, Self-powered acceleration sensor based on liquid metal triboelectric nanogenerator for vibration monitoring, ACS Nano 11 (2017) 7440–7446.
[41] G. Liu, J. Chen, Q. Tang, L. Feng, H. Yang, J. Li, Y. Xi, X. Wang, C. Hu, Wireless electric energy transmission through various isolated solid media based on triboelectric nanogenerator, Adv. Energy Mater. 8 (2018) 1703086.
[42] J. Chen, H. Guo, X. He, G. Liu, Y. Xi, H. Shi, C. Hu, Enhancing performance of triboelectric nanogenerator by filling high dielectric nanoparticles into sponge PDMS film, ACS Appl. Mater. Interfaces 8 (2016) 736–744.
[43] H. Guo, M. Yeh, Y. Zi, Z. Wen, J. Chen, G. Liu, C. Hu, Z.L. Wang, Ultralight cut-paper-based self-charging power unit for self-powered portable electronic and medical systems, ACS Nano 11 (2017) 4475–4482.
[44] J. Chen, H. Guo, G. Liu, X. Wang, Y. Xi, M. Javed, C. Hu, A fully-packaged and robust hybridized generator for harvesting vertical rotation energy in broad frequency band and building up self-powered wireless systems, Nano Energy 33 (2017) 508–514.
[45] J. Luo, Z.L. Wang, Recent advances in triboelectric nanogenerator based self-charging power systems, Energy Storage Mater. (2019) 2405–8297.
[46] H. Guo, X. Pu, J. Chen, Y. Meng, M. Yeh, G. Liu, Q. Tang, B. Chen, D. Liu, S. Qi, Song, C. Wu, C. Hu, J. Wang, Z.L. Wang, A highly sensitive, self-powered triboelectric auditory sensor for social robotics and hearing aids, Sci. Robot. 3 (2018) eaat2516.
[47] Y. Xi, H. Guo, Y. Zi, X. Li, J. Wang, J. Deng, S. Li, C. Hu, X. Cao, Z.L. Wang, Multifunctional TENG for blue energy scavenging and self-powered wind-speed sensor, Adv. Energy Mater. 7 (2017) 1–6.
[48] Y. Xie, J. Long, P. Zhao, J. Chen, J. Luo, Z. Zhang, K. Li, Y. Han, X. Hao, Z. Qu, M. Lu, W. Yin, A self-powered radio frequency (RF) transmission system based on the combination of triboelectric nanogenerator (TENG) and piezoelectric element for disaster rescue/relief, Nano Energy 54 (2018) 331–340.
[49] Y. Wu, X. Zhong, X. Wang, Y. Yang, Z.L. Wang, Hybrid energy cell for simultaneously harvesting wind, solar, and chemical energies, Nano. Res. 7 (2014) 1631–1639.
[50] J. Wang, C. Wu, Y. Dai, Z. Zhao, A. Wang, T. Zhang, Z.L. Wang, Achieving ultrahigh triboelectric charge density for efficient energy harvesting, Nat. Commun. 8

(2017) 88.
[51] T. Jiang, X. Chen, C.B. Han, W. Tang, Z.L. Wang, Theoretical study of rotary free-standing triboelectric nanogenerators, Adv. Funct. Mater. 25 (2015) 2928–2938.
[52] X. Liang, T. Jiang, G. Liu, T. Xiao, L. Xu, W. Li, F. Xi, C. Zhang, Z.L. Wang, Triboelectric nanogenerator networks integrated with power management module for water wave energy harvesting, Adv. Funct. Mater. (2019) 1807241.
[53] C. Xu, Y. Zi, A.C. Wang, H. Zou, Y. Dai, X. He, P. Wang, Y.C. Wang, P. Feng, D. Li, Z.L. Wang, On the electron-transfer mechanism in the contact-electrification effect, Adv. Mater. 30 (2018) 1706790.

Asif Abdullah Khan received his B.Sc degree in Electrical and Electronic Engineering, from Khulna University of Engineering and Technology (KUET), Bangladesh. During his bachelor degree, his research was focused on III-nitride material based semiconductor devices, and their modeling and characterization. From, 2018 he started pursuing his Ph.D. in Electrical and Computer Engineering at University of Waterloo, under the supervision of Prof. Dayan Ban. His research focuses on synthesis and characterization of novel nanomaterials, utilizing piezoelectric/triboelectric/synergistic effects for energy harvesting applications, self-powered electronics, and IoT.

Alam Mahmud is currently working as a research assistant in the department of Electrical and Computer Engineering at the University of Waterloo, and his research interests include but not limited to biotemplated novel nano materials synthesis and characterization, nanofabrication, nano biosensors, bioelectronics, brain-machine interfaces, nanometer-sized systems or particles for lab-on-the-chip technologies. He received his MASc in Electrical and Computer Engineering – Nanotechnology from the University of Waterloo under the supervision of Prof. Dayan Ban and BSc in Electrical and Electronic Engineering from Bangladesh University of Engineering and Technology (BUET). He will be joining the Ph.D. program in the Edward S. Rogers Sr. Department of Electrical & Computer Engineering, University of Toronto, under the supervision of Prof. Ted Sargent and will be working on wearable nanobiosensors for healthcare monitoring

Steven Zhang is working as a research associate in the department of Electrical and Computer Engineering at the University of Waterloo. He is an experienced senior system design engineer and posses the license of Professional Engineers Ontario. He has been working on wearable health monitoring products and system design with various sensors under industry environments.

Dr. Shariful Islam is working as a Manager, R & D and Special Projects at Shimco North America Inc. He received his B.Sc. in Mechanical Engineering from Bangladesh University of Engineering and Technology (2001), M. A. Sc. in Mechanical Engineering from Dalhousie University (2009), M. A. Sc. in Industrial Engineering from Dalhousie University (2014), and Ph.D. in Engineering from the University of Guelph (2017). Dr. Islam is also a visiting scholar in the Department of Electrical & Computer Engineering at the University of Waterloo. His research interests include modeling of advanced clean energy conversion devices, feedback control system, MEMS, and nanotechnology.

Peter Voss earned his Bachelor of Science in Physics from McMaster University in 1988 and went on to earn his CPA at Price Waterhouse. After several senior positions at hi-tech companies in Canada, Peter purchased and manages Shimco, a hi-tech aerospace manufacturing company in Ontario, Canada. Peter recognized a need to make products in aerospace safer and more intelligent, so he formed a team at Shimco to work with local research institutions to develop technologies to address that need. Peter and his team have projects currently with the University of Waterloo, the University of Guelph and McMaster University.

Dr. Dayan Ban is a professor in the Department of Electrical and Computer Engineering at the University of Waterloo. Dayan Ban earned BASc, MASc degrees at the University of Science and Technology of China, Hefei, China in 1993 and 1995, respectively and PhD degree at the University of Toronto in 2003. He spent his sabbatical leave at the Research Laboratory of Electronics (RLE) at MIT, cambridge, MA, USA in 2009 as a visiting scientist. He was a research staff at the Institute for Microstructural Sciences of National Research Council, Ottawa, Canada, before joining the University of Waterloo in 2005. He was a visiting scientist in 2001–2002 at Nortel, where he and his colleagues developed and applied novel scanning probe microscopy techniques. His current research interests include Optoelectronics, semiconductor quantum devices, terahertz quantum cascade lasers, infrared optical up conversion devices, Infrared imaging devices, scanning probe microscopy, nanotechnology and nanofabrication.